DOI: 10.1021/ic900302a

Inorganic Chemistry
Article

$Zn_5Sb_4In_{2-\delta}$ — a Ternary Derivative of Thermoelectric Zinc Antimonides

Yang Wu,[†] Sven Lidin,[‡] Thomas L. Groy,[†] N. Newman,[§] and Ulrich Häussermann*[,†]

[†]*Department of Chemistry and Biochemistry, Arizona State University, Tempe, Arizona 85287-1604,* [‡]*Inorganic Chemistry, Stockholm University, SE-10691 Stockholm, Sweden, and* [§]*School of Materials, Arizona State University, Tempe, Arizona 85287-8706*

Received February 16, 2009

$Zn_5Sb_4In_{2-\delta}$ (δ = 0.15(3)) was synthesized in the form of millimeter-sized crystals from reaction mixtures containing excess zinc. The ternary intermetallic compound is temperature polymorphic, and at room temperature it crystallizes with a new structure type in the orthorhombic space group *Pbcn*, where a = 7.1619(2), b = 17.1562(4), c = 8.6887(4) Å, V = 1067.6(1) Å^3, and Z = 4. The structure features 3^2434 nets of Sb atoms that are stacked in antiposition to yield layers of square antiprisms sharing edges plus intervening tetracapped tetrahedra (tetreadersterns). The majority of Zn atoms occupy peripheral tetrahedra of such tetraedersterns, and attain at the same time the peculiar five-coordination by one like atom and four Sb atoms typical for the structures of binary zinc antimonides. The In and remaining Zn atoms are distributed in the tetragonal channels formed by the square antiprisms and display some disorder. At temperatures below 200 K $Zn_5Sb_4In_{2-\delta}$ undergoes a phase transition into a more ordered structure with monoclinic symmetry ($P2_1/c$) without any change of the unit cell. The thermoelectric properties of $Zn_5Sb_4In_{2-\delta}$ were measured between 10 and 350 K. Exceptionally low thermal conductivity values (1 W/mK range) were obtained in the whole temperature range. Resistivity and thermopower values are characteristic of a heavily doped or degenerate semiconductor (2.5 mΩ cm and 160 μV/K, respectively, at room temperature) and show a discontinuity around 220 K. The thermoelectric figure of merit of $Zn_5Sb_4In_{2-\delta}$ is higher than that of Zn_4Sb_3 in the investigated temperature range.

1. Introduction

Binary zinc antimonides have been intensively investigated for their thermoelectric properties.[1−7] This holds especially true for Zn_4Sb_3, which displays an exceptionally low thermal conductivity and high thermoelectric figures of merits between 450 and 670 K.[8] The characteristic and peculiar feature of zinc antimonides are their weakly polar, rather complex framework structures combined with a narrow band gap at or close to the Fermi level.[9]

The Zn−Sb system affords three fields of phases which are located in the narrow range between 50 and 60 at.% Zn.[10,11] ZnSb is a stoichiometric compound with a well characterized crystal structure (CdSb type).[12] Zn_4Sb_3 displays complex temperature polymorphism.[13−16] The room temperature (RT) form, β-Zn_4Sb_3, undergoes two consecutive phase transitions at low temperatures (between 235 and 255 K) and a transition to high-temperature γ-Zn_4Sb_3 at approximately 765 K.[17] Zn_3Sb_2 is metastable and appears in a low-temperature (between 677 and 714 K) and high-temperature form (between 714 and 841 K), which both can be quenched to RT. The structures and exact compositions of the Zn_4Sb_3 and Zn_3Sb_2 phases have been controversial for a long time. Only lately β-Zn_4Sb_3 was recognized as heavily disordered,

*To whom correspondence should be addressed. E-mail: ulrich.haussermann@asu.edu.

(1) Nolas, G. S.; Poon, J.; Kanatzidis, M. *MRS Bull.* **2006**, *31*, 199–205.
(2) Xu, J. X.; Kleinke, H. *J. Comput. Chem.* **2008**, *29*, 234.
(3) Ur, S. C.; Kim, I. H.; Nash, P. *J. Mater. Sci.* **2007**, *42*, 2143.
(4) Nakamoto, G.; Akai, N.; Kurisu, M. *J. Alloys Compd.* **2007**, *437*, 151.
(5) Pedersen, B. L.; Iversen, B. B. *Appl. Phys. Lett.* **2008**, *92*, 161907.
(6) Goncharuk, L. V.; Lukashenko, G. M. *Inorg. Mater.* **1989**, *25*, 1621.
(7) Shaver, P. J.; Blair, J. *Phys. Rev.* **1966**, *141*, 649.
(8) Caillat, T.; Fleurial, J.-P.; Borshchevsky, A. *J. Phys. Chem. Solids* **1997**, *58*, 1119.
(9) Mikhaylushkin, A. S.; Nylén, J.; Haussermann, U. *Chem.—Eur. J.* **2005**, *17*, 4912.
(10) Massalski, T. S. *Binary Alloy Phase Diagrams*, 2nd ed.; American Society for Metals: Metals Park, OH, 1990.
(11) Izard, V.; Record, M. C.; Tedenac, J. C.; Fries, S. G. *Chalpad* **2001**, *25*, 567.
(12) Almin, K. E *Acta Chem. Scand.* **1948**, *2*, 400.
(13) Ugai, Y. A.; Marshakova, T. A.; Shevchenko, V. Y.; Demina, N. P. *Izv. Akad. Nauk SSSR, Neorg. Mater.* **1969**, *5*, 1381.
(14) Shevchenko, V. Y.; Skripkin, V. A.; Ugai, Y. A.; Marshakova, T. A. *Izv. Akad. Nauk. SSSR, Neorg. Mater.* **1968**, *4*, 1359.
(15) Souma, T.; Nakamoto, G.; Kurisu, M. *J. Alloys Compd.* **2002**, *340*, 275.
(16) Mozharivskyj, Y.; Janssen, Y.; Harringa, J. L.; Kracher, A.; Tsokol, A. O.; Miller, G. J. *Chem. Mater.* **2006**, *18*, 822.
(17) Mozharivskyj, Y.; Pecharsky, A. O.; Bud'ko, S.; Miller, G. J. *Chem. Mater.* **2004**, *16*, 1580.

Published on Web 05/28/2009

displaying a high concentration of interstitial Zn atoms, which provided a ready explanation for its low thermal conductivity.[18−20] Further, the complex structures of ordered α- and α′-Zn_4Sb_3 ($Zn_{13-x}Sb_{10}$) could be characterized,[21−23] and the structure of high-temperature Zn_3Sb_2 has been identified as incommensurately modulated with the modulation vector coupled to a small homogeneity range $Zn_{3-x}Sb_2$ ($0.167 < x < 0$).[24]

The peculiar structural and electronic properties of zinc antimonides raises the question whether there are derivatives, or related systems, which would allow to embed zinc antimonides into a larger family of compounds. Furthermore, the identification of derivatives would assist in establishing more detailed structure−property correlations and consequently help toward a deeper understanding of the origin of the thermoelectric properties in these materials.

Recently we reported on metastable Cd_4Sb_3, which in terms of structural properties is rather similar to Zn_4Sb_3 and also displays an extraordinarily low thermal conductivity.[25] Especially, in both systems the occurrence of disordered, interstitial atoms that are susceptible to temperature dependent ordering is a characteristic feature. Furthermore, we found a ternary derivative, $Cd_{13-x}In_ySb_{10}$, where trivalent indium appears to replace a considerable concentration of divalent cadmium.[26] This results in an interstitial-free framework structure, where the electron concentration is essentially maintained with respect to Cd_4Sb_3 but properties are radically changed. Similar attempts in the Zn−Sb−In system led to a different result. In contrast to the Cd−Sb−In system, indium does not produce a substitutional variant of a known zinc antimonide structure, but segregates into distinct crystallographic positions in new, ternary, crystal structures. The exploration of the Zn−Sb−In system yielded hitherto two new phases, $Zn_5Sb_4In_{2-\delta}$ and $Zn_9In_6In_2$, with similar structures. Herein we report on the synthesis, structure, and property characterization of $Zn_5Sb_4In_{2-\delta}$.

2. Experimental Section

Synthesis and Phase Characterization. All samples for the synthesis were prepared in a dry-argon filled glovebox. Pure Zn (granules, 99.99%), Sb (powder, 99.5%), and In (ingot, 99.99%) were purchased from Sigma-Aldrich. $Zn_5Sb_4In_{2-\delta}$ specimens used for crystal structure analysis and property measurements were prepared from a starting molar composition of Zn:Sb:In = 5:2:3. Powdered Sb was pressed into a pellet and all starting metals were loaded into silica tubes specially prepared for flux synthesis.[27] After flame sealing under vacuum ($< 10^{-5}$ bar) ampules were placed into a well insulated stainless-steel container. The reaction was carried out in a box furnace with a programmable temperature controller. First, the temperature was raised to 923 K and kept for 24 h to homogenize the metal mixture. Subsequently the temperature was lowered to 623 K at rates between 2 and 5 K/h, and the reaction mixture held at this temperature for 100 h. This procedure resulted in millimeter-sized, often agglomerated crystals of $Zn_5Sb_4In_{2-\delta}$ which were separated from the liquid excess metal mixture by centrifugation. The intermetallic compound is air and moisture stable.

For phase analysis, powder X-ray diffraction patterns were collected on a Siemens D5000 diffractometer (Cu Kα radiation), and the composition of the products was analyzed by electron probe microanalysis (EPMA) in a JEOL JXA-8600 microscope operated at 15.0 kV and 30.0 nA. Specimens were enclosed in epoxy and polished. Elemental metals were used as standards for Sb and Zn, while InSb was used for In. The ZAF correction procedure was employed for quantitative composition determination.

Crystal Structure Characterization. Crystals suitable for single crystal X-ray diffraction were obtained by crushing a large crystal specimen obtained by flux synthesis. Intensity data collection was performed at RT (295 K), 200, 150, and 120 K on an Oxford Diffraction Xcalibur 3 CCD diffractometer with monochromatic Mo Kα radiation ($\lambda = 0.71073$ Å) operated at 50 kV and 40 mA and equipped with an Oxford cryo system cooler. The sample-to-detector distance was 50 mm. Oxford Diffraction's CrysAlis software was employed for data reduction.[28]

The diffraction patterns can be indexed in a orthorhombic unit cell ($a \approx 7.15$ Å, $b \approx 17.15$ Å, $c \approx 8.7$ Å). The RT measurement shows unambiguously systematic extinctions in the Bragg reflections compatible with the space group *Pbcn*. At 120 K the n-glide perpendicular to *c* and the c-glide perpendicular to *b* are both violated by many reflections, suggesting ordering in a subgroup to *Pbcn*. Centro-symmetric orthorhombic groups allow for two different kinds of maximal non-isomorphic subgroups, non-centric orthorhombic with the possible point group symmetries mm2, m2m, 2mm, and 222 and centro-symmetric monoclinic with the point group symmetries 2/m11, 12/m1, and 112/m respectively. As two out of three of the glide planes are disallowed in the low temperature data, only two of these maximal subgroups are compatible with the extinction conditions, namely, those with point group symmetries 222 ($P2_12_12$ in standard setting) and 2/m11, ($P2_1/c$ in standard setting). The strict adherence to the b-glide perpendicular to *a* (i.e., the c-glide perpendicular to *b* in standard setting) and the violation of the 2-fold screw axis along *c* is a strong indication that the centro-symmetric monoclinic group $P2_1/c$ is the proper choice.

The structures of both the RT phase and the low temperature (LT) phase were solved by charge flipping, using the program Superflip.[29] The models were refined against F^2 data using the program JANA2000.[30] In the final refinements, Sb and Zn positions were considered to be fully occupied, while the occupancies of the In positions were refined. A model of the disordered RT phase refines to 0.053/0.138 R1/wR2 for *all* reflections. For the LT phase it is possible to refine an ordered, twinned, model in S.G. $P2_1/c$ to an agreement 0.042/0.121 R1/wR2 for *all* reflections. The applied twinning matrix (pseudo-orthorhombic cell) was (1 0 0, 0 1 0, 0 0 −1). Table 1 lists a summary of the refinement results. Details are supplied as Supporting Information, or can be obtained from the Fachinformationszentrum Karlsruhe, 76344 Eggenstein-Leopoldshafen,

(18) Snyder, G. J.; Christensen, M.; Nishibori, E.; Caillat, T.; Iversen, B. B. *Nat. Mater.* **2004**, *3*, 458.
(19) Cargnoni, F.; Nishibori, E.; Rabiller, P.; Bertini, L.; Snyder, G. J.; Christensen, M.; Gatti, C.; Iversen, B. B. *Chem.—Eur. J.* **2004**, *10*, 3862.
(20) Toberer, E. S.; Sasaki, K. A.; Chisholm, C. R. I.; Haile, S. M.; Goddard, W. A.; Snyder, G. J. *Phys. Status Solidi RRL* **2007**, *1*, 253.
(21) Nylén, J.; Andersson, M.; Lidin, S.; Häussermann, U. *J. Am. Chem. Soc.* **2004**, *126*, 16306.
(22) Nylén, J.; Lidin, S.; Andersson, M.; Iversen, B. B.; Liu, H. X.; Newman, N.; Häussermann, U. *Chem. Mater.* **2007**, *19*, 834.
(23) Nylén, J.; Lidin, S.; Andersson, M.; Liu, H.; Newman, N.; Häussermann, U. *J. Solid State Chem.* **2007**, *180*, 2603.
(24) Boström, M.; Lidin, S. *J. Alloys Compd.* **2004**, *376*, 49.
(25) Tengå, A.; Lidin, S.; Belieres, J.-P.; Newman, N.; Wu, Y.; Häussermann, U. *J. Am. Chem. Soc.* **2008**, *130*, 15564.
(26) Tengå, A.; Lidin, S.; Belieres, J.-P.; Newman, N.; Wu, Y.; Häussermann, U. *Chem.—Eur. J.* **2009**, in press, DOI: 10.1002/chem.200802695.
(27) Boström, M.; Hovmöller, S. *J. Solid State Chem.* **2000**, *153*, 398.
(28) *CrysAlis, Software for automated data collection and reduction*; Oxford Diffraction: Oxford, U.K., 2006.
(29) Palatinus, L.; Chapuis, G. *J. Appl. Crystallogr.* **2007**, *40*, 786.
(30) Petricek, V.; Dusek, M. *The crystallographic computing system JANA2000*; Institute of Physics: Praha, Czech Republic, 2000.

Table 1. Selected Crystallographic Data for RT and LT $Zn_5Sb_4In_{1.85(3)}$

	RT	LT
formula	$Zn_{20}Sb_{16}In_{7.5}$	$Zn_{20}Sb_{16}In_{7.5}$
formula weight	1029.6	1029.6
crystal size, mm^3	$0.049 \times 0.063 \times 0.089$	$0.049 \times 0.063 \times 0.089$
space group	*Pbcn* (No. 60)	$P2_1/c$ (No.14)
a, Å	7.1619(2)	8.6518(2)
b, Å	17.1562(4)	7.1360(4)
c, Å	8.6887(4)	17.1158(4)
β, deg		90
Z; *V*, $Å^3$	1;1067.59(6)	1;1056.72(7)
D_{calc}, g cm^{-3}	6.3783	6.475
temp, K	293 K	120 K
λ(Mo Kα), Å	0.71069	0.71069
absorption coeff, mm^{-1}	25.119	25.119
F(000)	1777	1784
θ_{min}-θ_{max}, deg	3.87−30.89	3.70−30.84
index ranges	$-9 \le h \le 10$	$-12 \le h \le 12$
	$-24 \le k \le 24$	$-10 \le k \le 9$
	$-12 \le l \le 12$	$-24 \le l \le 24$
total reflns collected	15534	16233
independent reflns	1622 [*R*(int) = 0.0328]	3067 [*R*(int) = 0.0283]
refinement method	full-matrix least-squares on F^2	full-matrix least-squares on F^2
data/restraints/params	1622/0/59	3067/0/104
final *R* indices [$I > 3\sigma(I)$][a,b]	$R_1 = 0.0391$	$R_1 = 0.0356$
	$wR_2 = 0.1267$	$wR_2 = 0.1173$
R indices (all data)[a,b]	$R_1 = 0.0529$	$R_1 = 0.0416$
	$wR_2 = 0.1379$	$wR_2 = 0.1213$
largest diff, peak and hole, e $Å^{-3}$	2.32 and −1.62	1.81 and −1.49
GOF on F^2	1.41	1.31

[a] $R_1 = \sum||F_o| - |F_c||/\sum|F_o|$. [b] $wR_2 = [\sum w(F_o^2 - F_c^2)^2/\sum w(F_o^2)^2]^{1/2}$.

Germany, (fax: (49) 7247−808−666; e-mail: crysdata@fiz-karlsruhe.de) on quoting the depository numbers CSD-420363 (295 K) and CSD-420364 (120 K).

Physical Property Measurements. The electrical resistivity, thermopower and thermal conductivity of $Zn_5Sb_4In_{2-\delta}$ were measured on a Physical Property Measurement System (PPMS) from Quantum Design equipped with the Thermal Transport Option (TTO). A brick-like crystal was selected and carefully shaped and polished into a rectangular block with dimensions of $4.53 \times 1.17 \times 2.21$ mm^3. The surface of the obtained specimen was free from any excess metal residual from the flux synthesis. For the thermal transport, two copper disks with extruded leads on each end were glued oppositely onto the specimen using a two-component silver-filled epoxy (Epo-Tek H20E), which provided contact after curing at slightly elevated temperatures for a short time. The arrangement was then mounted on the TTO puck, which was subsequently loaded into the PPMS chamber and then evacuated to high vacuum ($< 10^{-3}$ torr) for the measurement. The thermal transport measurements were conducted in a two-point configuration from 10 to 350 K at a scanning rate of 0.3 K/min. At a certain temperature, a heat pulse was applied to the sample to create a temperature gradient. Thermal conductivity and Seebeck coefficient were obtained when the sample was equilibrated. The autorange feature was used in all of the measurements in the PPMS system. Radiation heat loss was automatically corrected with the incorporated functions of the software. More accurate resistivity was acquired with a 4-probe in-line configuration using the Resistivity Option on the same PPMS by introducing up to a maximum value of 1 mA DC current. Single cooling and cooling−heating measurements from 10 to 350 K were performed at a rate of 1 K/min, respectively.

3. Results and Discussion

Synthesis and Phase Analysis of $Zn_5Sb_4In_{2-\delta}$. A systematic study of the Zn-rich corner of the ternary phase diagram Zn−Sb−In afforded two new phases, $Zn_5Sb_4In_{2-\delta}$ and $Zn_9Sb_6In_2$. $Zn_9Sb_6In_2$ decomposes already at around 600 K into $Zn_5Sb_4In_{2-\delta}$, Zn_4Sb_3, and Zn, but can be obtained by rapidly quenching ternary melts.[31] $Zn_5Sb_4In_{2-\delta}$ forms together with Zn_4Sb_3 and InSb when stoichiometric melts are slowly cooled, which indicates that $Zn_5Sb_4In_{2-\delta}$ melts incongruently. When employing flux conditions by using excess Zn and In metal the byproducts are suppressed, and $Zn_5Sb_4In_{2-\delta}$ is obtained in the form of millimeter-sized crystals. Figure 1 summarizes the applied reaction mixtures used and corresponding temperatures where flux conditions are maintained. Additionally the products are indicated.

The X-ray powder pattern of $Zn_5Sb_4In_{2-\delta}$ can be indexed in an orthorhombic unit cell and no significant shifts of peak positions are observed for products obtained from different starting compositions. EPMA analysis yielded a composition 46.8(3) at.% Zn, 35.7(3) at.% Sb, and 17.5(1) at.% In. The elemental composition of $Zn_5Sb_4In_{2-\delta}$ did not vary significantly for crystal specimens from the same sample, and between specimens from samples obtained from different starting compositions or from applying different flux temperatures. The results from X-ray powder diffraction and electron probe microanalysis suggest that $Zn_5Sb_4In_{2-\delta}$ has no or only a very small homogeneity range. Differential Scanning Calorimetry scans from RT to 853 K show that $Zn_5Sb_4In_{2-\delta}$ undergoes several high temperature phase transitions

(31) Wu, Y.; Tengå, A.; Lidin, S.; Häussermann, U., unpublished results. X-ray diffraction data for $Zn_9Sb_6In_2$ were collected at RT on an Oxford Diffraction Xcalibur 3 CCD diffractometer with monochromatic Mo Kα radiation. The structure was solved by charge flipping[29] and refined using JANA2000[30]. Obtained crystallographic data are orthorhombic, $P2_12_12_1$, $Z = 8$, $a = 7.1416(6)$, $b = 17.1463(9)$, $c = 25.719(2)$, 7183 independent reflections, 1808 reflections with $I > 3\sigma(I)$, R1 = 0.0554.

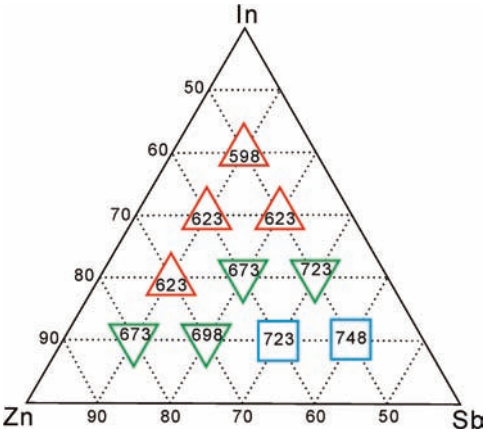

Figure 1. Synthesis diagram for $Zn_5Sb_4In_{2-\delta}$. Colored symbols mark employed compositions with temperatures inscribed that are necessary for maintaining flux conditions. Red (upward triangles), $Zn_5Sb_4In_{2-\delta}$ with traces of InSb; green (downward triangles), product mixture of $Zn_5Sb_4In_{2-\delta}$ and Zn_4Sb_3; blue (squares), Zn_4Sb_3. Compositions on axes are in at.%.

above 573 K and decomposes at a temperature between 750 and 800 K.

Crystal Structure of $Zn_5Sb_4In_{2-\delta}$. The RT form of $Zn_5Sb_4In_{2-\delta}$ crystallizes with the orthorhombic space group *Pbcn* and contains seven distinct atomic positions (Figures 2 and 3, Tables 1−3). Zn1, Zn2, Sb1, and Sb2 atoms are situated on general sites 8d, while In1 and In2 atoms occupy sites 4c. The In positions display some occupational deficiency (5−10%) which is indicated as δ in the compound formula. The Zn3 position represents a split position (i.e., a half occupied general position 8d). The refined composition of $Zn_5Sb_4In_{2-\delta}$ is $Zn_5Sn_4In_{1.85(3)}$ (δ = 0.15(3)).

The characteristic feature of the $Zn_5Sb_4In_{2-\delta}$ structure are 3^2434 nets formed by the Sb atoms that are stacked in antiposition orientation along the *a* direction. This yields rows of face-sharing square antiprisms that are connected in the *bc* plane by sharing triangle edges. Such an arrangement of 3^2434 nets occurs in many intermetallic compounds, most prominent is probably the $CuAl_2$ type where nets are formed by Al atoms while Cu atoms center square antiprisms.[32] The arrangement of Sb atoms is body centered tetragonal (its unit cell is indicated in Figure 2a) and contains also intervening tetracapped tetrahedra usually termed tetreadersterns (Figure 2b).[32] In some stuffed variants of the $CuAl_2$ type the center of the central tetrahedron is occupied which retains the tetragonal symmetry (e.g., in "TlSe" larger Tl^+ and smaller Tl^{3+} occupy square antiprims and central tetrahedra, respectively).

In $Zn_5Sb_4In_{2-\delta}$, however, Zn1 and Zn2 occupy two of the four peripheral tetrahedra in Sb_8 tetreadersterns. Those peripheral tetrahedra are adjacent which results in rather short distances Zn1−Zn1 and Zn2−Zn2 (below 3 Å). The distribution of Zn atoms (or "Zn pairs") is shown in Figure 2c with three tetreadersterns that are consecutively stacked along the *a* direction and in Figure 2a where different colors denote different heights along *a*. It results in a symmetry lowering of the originally

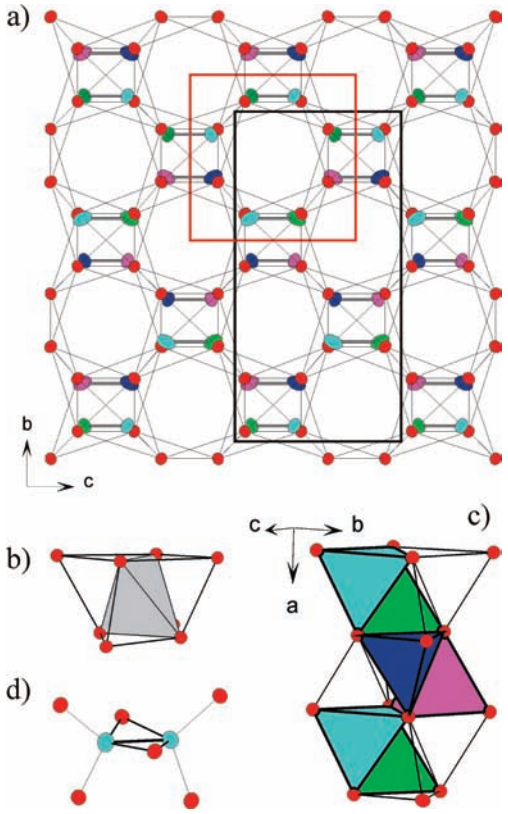

Figure 2. Framework "ZnSb" in $Zn_5Sb_4In_{2-\delta}$. (a) Sb atoms (red circles) form 3^2434 nets (thin lines) stacked in antiposition along the *a* direction. The unit cell of the Sb atom arrangement is outlined in red, the one of the $Zn_5Sb_4In_{2-\delta}$ structure in black. (b) Tetracapped tetrahedron ("tetraedersterns") formed by eight Sb atoms. The central tetrahedron (empty) is marked in gray. (c) Arrangement of tetraedersterns in $Zn_5Sb_4In_{2-\delta}$ with peripheral tetrahedra occupied by Zn atoms. Different colors indicate different heights in the *a* direction (cf. (a) where pairs of Zn atoms are connected by gray, thick, lines). Cyan $x \approx 0.12$; Green $x \approx 0.38$; Blue $Hx \approx 0.62$; Purple $x \approx 0.88$. (d) Coordination environment of Zn atoms. Rhomboid rings Zn_2Sb_2 are emphasized with bold lines. Ellipsoids are drawn at a 90% probability.

tetragonal arrangement of Sb atoms to orthorhombic and a doubling of the unit cell. It should be noted that the kind of distribution of Zn atoms in tetraedersterns is unusual when considering the structure of $Zn_5Sb_4In_{2-\delta}$ as a derivative of the $CuAl_2$ type. None of the ubiquitous structures based on antiposition stackings of 3^2434 nets and different fillings of square antiprisms and tetrahedra display this kind of distribution.[33] However, the Zn distribution yields a structural fragment characteristic for binary zinc antimonides, namely, rhomboid rings Zn_2Sb_2 as a part of face sharing tetrahedra $ZnSb_4$.[9] As in binary zinc antimonides, Zn atoms in $Zn_5Sb_4In_{2-\delta}$ (Zn1 and Zn2) display a peculiar 5-coordination by one like atom and four Sb atoms (Figure 2d).

The framework of Sb and Zn1 and Zn2 atoms represents a (2 × 1 × 1) superstructure with respect to the tetragonal basis structure of Sb atoms. It has a composition ZnSb and involves 32 atoms in the unit cell. The remaining atoms (In1, In2, and Zn3) are located in the channels provided by the rows of square antiprisms (Figure 3a). The stuffing of those channels in

(32) Hyde, B.; Andersson, S. *Inorganic Crystal Structures*; John Wiley & Sons: New York, 1989.

(33) Villars, P.; Calvert, L. D. *Pearsons Handbook of Crystallographic Data for Intermetallic Compounds*, 2nd ed.; ASM International: Materials Park, OH, 1991; Desk Edition 1997.

RT-$Zn_5Sb_4In_{2-\delta}$ does not result in any further symmetry lowering. Centers of square antiprisms are occupied alternately by pairs of Zn3 and In1 atoms, and single In2 atoms. Their coordination is shown in Figure 3b. The distance between pairs of Zn3 and In1 atoms is peculiarly short, 2.62 Å. In2 atoms have large and anisotropic displacement parameters (see Supporting Information) and appear loosely coordinated by the eight Sb atoms forming the square antiprism and additionally six Zn atoms. Furthermore the two pairs Zn3−In1 located in neighboring square antiprisms can also be considered coordinating In2 (not shown in Figure 3b). The nearest neighbor distances vary continuously from 3.4 to 3.85 Å. The smallest distance is to Zn2 atoms. The Zn3 split position and the occupational deficiency of In atoms indicate disorder within the tetragonal channels formed by the square antiprisms. Also, the composition from the microprobe analysis (46.3% Zn; 35.7% Sb; 17.5% In) suggests a slightly higher Zn/Sb ratio compared to the crystallographically refined one (45.9% Zn; 36.7% Sb; 17.3% In).

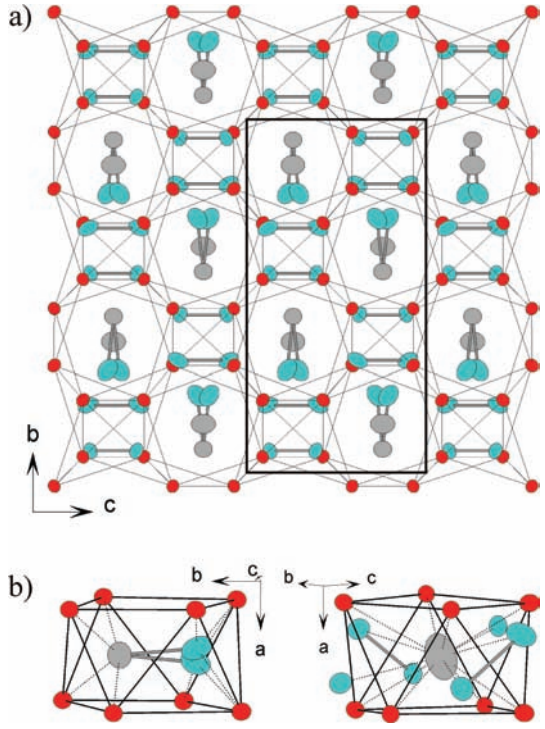

Figure 3. (a) Total structure of $Zn_5Sb_4In_{2-\delta}$ projected along the *a* direction. Cyan, red, and gray ellipsoids denote Zn, Sb, and In atoms, respectively. Atom pairs Zn−Zn and Zn−In are connected by gray, thick, lines. (b) Coordination environment (broken lines) of atoms centering Sb_8 square antiprisms (solid lines). Left: Zn3−In1 pair, right: In2 atom. Ellipsoids are drawn at a 90% probability.

At low temperatures (below 200 K) $Zn_5Sb_4In_{2-\delta}$ undergoes a structural phase transition. Additional reflections appear that violate the extinction conditions imposed by the n- and c-glide planes in *Pbcn* (Figure 4a). The symmetry is lowered to monoclinic without any change in the unit cell. In space group $P2_1/c$ the split position resolves into a single 4-fold Zn position (Zn3). As a consequence, pairs Zn−In within tetragonal channels that were previously arranged parallel to the orthorhombic *b* axis are now slightly tilted with respect to this axis (the monoclinic *c* axis). This is shown in Figure 4b. Apart from that, the structure remains virtually unchanged.

The structural behavior of $Zn_5Sb_4In_{2-\delta}$ is strongly reminiscent of binary Zn_4Sb_3. Here the RT phase (β-Zn_4Sb_3; S.G. $R\bar{3}m$) is substantially disordered which is manifested in interstitial Zn atoms distributed on three weakly occupied (to about 5%) general sites 36f.[18,19] Upon cooling Zn_4Sb_3 undergoes two phase transitions to the consecutively higher ordered phases α and α′ where interstitial Zn atoms occupy distinct crystallographic sites in highly complex low-symmetry crystal structures.[21−23] One could suspect that the deviation between microprobe determined and crystallographic composition is caused by a small concentration of interstitial Zn atoms in $Zn_5Sb_4In_{2-\delta}$. When increasing the unit cell content from 20 to 21 Zn atoms (i.e., by 5%) a good agreement is obtained. However, we did not find any clear evidence for weakly occupied Zn positions in our refinements. Instead, we propose that crystals of $Zn_5Sb_4In_{2-\delta}$ contain domains of the phase $Zn_9Sn_6In_2$, which has a higher Zn content.

The crystal structures of $Zn_9Sb_6Sb_2$ and $Zn_5Sb_4In_{2-\delta}$ have identical ZnSb frameworks (cf. Figure 2a) but differ in the stuffing of the tetragonal channels. Instead of pairs

Table 2. Atomic Coordinates and Isotropic Displacement Parameters for RT and LT $Zn_5Sb_4In_{1.85(3)}$

	atom	Wyck.	occ.	*x*	*y*	*z*	U_{iso} (Å^2)
RT	Zn1	8d	1	0.6134(1)	0.55866(6)	0.3776(1)	0.0207(3)
	Zn2	8d	1	0.6202(2)	0.18741(7)	0.1102(2)	0.0286(3)
	Zn3	8d	0.5	0.0377(4)	0.7141(2)	0.7820(4)	0.042(1)
	Sb1	8d	1	0.76445(7)	0.45854(3)	0.58049(6)	0.0142(2)
	Sb2	8d	1	0.74447(7)	0.29790(3)	0.91934(7)	0.0160(2)
	In1	4c	0.891(5)	0	0.56332(7)	0.75	0.0303(4)
	In2	4c	0.952(6)	0.5	0.36577(9)	0.25	0.0623(7)
LT	Zn1a	4e	1	0.8743(2)	0.3878(2)	0.55715(8)	0.0066(3)
	Zn1b	4e	1	0.6208(2)	0.61372)	0.55944(8)	0.0071(4)
	Zn2a	4e	1	0.8995(2)	0.8907(2)	0.68596(9)	0.0113(4)
	Zn2b	4e	1	0.3849(2)	0.6255(2)	0.81217(8)	0.0076(3)
	Zn3	4e	1	0.7055(2)	0.4498(2)	0.78468(9)	0.0179(4)
	Sb1a	4e	1	0.91867(9)	0.76582(9)	0.54075(5)	0.0046(2)
	Sb1b	4e	1	0.57851(9)	0.23652(9)	0.54207(5)	0.0046(2)
	Sb2a	4e	1	0.9207(1)	0.26164(9)	0.70132(5)	0.0058(2)
	Sb2b	4e	1	0.5864(1)	0.74664(9)	0.70320(5)	0.0052(2)
	In1	4e	0.919(4)	0.7552(1)	0.4932(1)	0.93596(5)	0.0105(2)
	In2	4e	0.960(6)	0.7462(2)	0.9783(3)	0.86476(5)	0.0246(3)

Table 3. Selected Interatomic Distances in Å[a] for RT and LT $Zn_5Sb_4In_{1.85(3)}$

atomic pair	distance	atomic pair	distance
	RT-$Zn_5Sb_4In_{2-\delta}$		
Zn1—Sb2	2.659(1)	Sb2—Zn1	2.659(1)
—Sb1	2.689(1)	—Zn2	2.671(1)
—Sb1	2.746(1)	—Zn3	2.706(3)
—Zn1	2.749(2)	—Zn2	2.715(1)
—Sb1	2.815(1)	—Zn3	2.752(3)
Zn2—Sb1	2.649(1)	—Zn2	2.867(1)
—Sb2	2.671(1)	—Zn3	3.035(3)
—Sb2	2.714(1)	In1—Zn3	2.616(3)
—Sb2	2.867(1)	—Sb1	2.8717(9)
—Zn2	2.978(2)	—Sb1	3.3516(6)
—Zn3	3.101(4)	—Zn1 × 2	3.644(1)
—Zn3	3.120(3)	—In2 × 2	3.7819(6)
Zn3—In1	2.616(3)	—Zn2 × 2	3.881(1)
—Sb2	2.706(3)	In2—Zn2 × 2	3.403(2)
—Sb2	2.752(3)	—Sb2	3.5603(7)
—Sb2	3.035(3)	—Zn1 × 2	3.579(1)
—Zn2	3.101(4)	—Zn1 × 2	3.583(2)
—Zn2	3.122(3)	—Zn3 × 2	3.594(3)
Sb1—Zn2	2.649(1)	—Sb2	3.660(1)
—Zn1	2.689(1)	—In1 × 2	3.7819(6)
—Zn1	2.746(1)	—Sb1	3.7902(8)
—Zn1	2.815(1)	—Sb1	3.852(1)
—In1	2.8717(9)		
	LT-$Zn_5Sb_4In_{2-\delta}$		
Zn1a—Sb2a	2.657(2)	Sb2a—Zn2a	2.644(2)
—Sb1a	2.687(2)	—Zn1a	2.657(2)
—Zn1b	2.722(2)	—Zn2a	2.666(1)
—Sb1a	2.739(1)	—Zn3	2.703(2)
—Sb1b	2.789(2)	—Zn2b	2.826(2)
Zn1b—Sb2b	2.654(2)	Sb2b—Zn1b	2.654(2)
—Sb1b	2.672(2)	—Zn2b	2.695(2)
—Zn1a	2.722(2)	—Zn2b	2.728(1)
—Sb1b	2.732(1)	—Zn3	2.738(2)
—Sb1a	2.815(2)	—Zn2a	2.913(2)
Zn2a—Sb2a	2.644(2)	—Zn3	2.919(2)
—Sb1a	2.646(2)	In1—Zn3	2.643(2)
—Sb2a	2.666(2)	—Sb1a	2.859(1)
—Sb2b	2.913(2)	—Sb1b	2.885(1)
—Zn2b	2.977(2)	—Sb1a	3.279(1)
Zn2b—Sb1b	2.637(2)	—Sb1b	3.390(1)
—Sb2b	2.695(1)	—Zn1a	3.571(2)
—Sb2b	2.728(1)	—In2	3.671(2)
—Sb2a	2.826(2)	—Zn1b	3.670(2)
—Zn3	2.952(2)	—Zn2a	3.717(2)
—Zn2a	2.977(2)	—In2	3.872(2)
—Zn3	3.080(2)	—Zn2b	3.956(2)
Zn3—In1	2.643(2)	In2—Zn2a	3.394(2)
—Sb2a	2.703(2)	—Zn2b	3.400(2)
—Sb2b	2.738(2)	—Sb2a	3.461(2)
—Sb2b	2.919(2)	—Sb2b	3.506(1)
—Zn2b	2.952(2)	—Zn1b	3.563(2)
—Zn2b	3.080(2)	—Zn1b	3.565(2)
Sb1a—Zn2a	2.646(2)	—Zn1a	3.604(2)
—Zn1a	2.687(2)	—Zn1a	3.604(2)
—Zn1a	2.739(1)	—Sb2b	3.647(2)
—Zn1b	2.815(2)	—Zn3	3.650(2)
—In1	2.859(1)	—Sb1b	3.662(2)
Sb1b—Zn2b	2.637(2)	—In1	3.671(2)
—Zn1b	2.671(2)	—Sb2a	3.768(1)
—Zn1b	2.732(1)	—Sb1a	3.786(1)
—Zn1a	2.789(2)	—In1	3.872(2)
—In1	2.885(1)	—Sb1a	3.903(2)
		—Sb1b	3.931(1)

[a] < 3.4 Å for Zn and Sb coordination, < 4.0 Å for In coordination.

Zn−In and single In atoms for $Zn_5Sb_4In_{2-\delta}$ triangles of Zn atoms and In atoms in a ratio 1:2 occur for $Zn_9Sb_6In_2$ (Figure 5).[31] As a consequence the unit cell *c* axis of

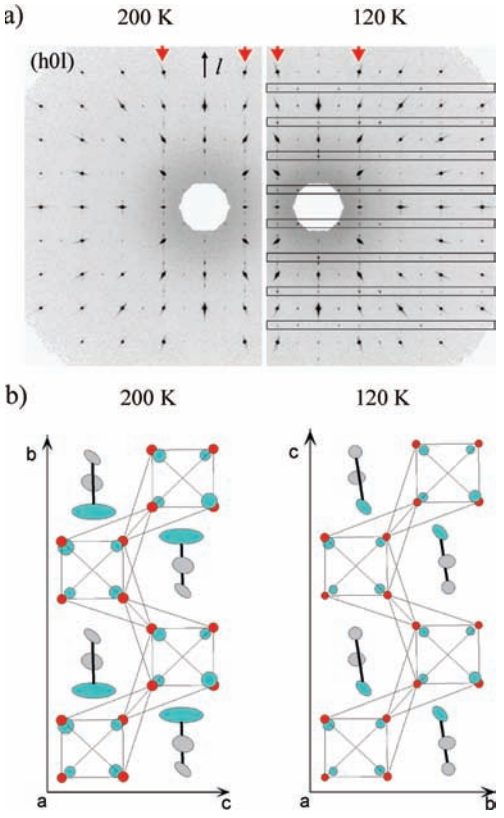

Figure 4. (a) Diffraction pattern of the (*h*0l) plane for $Zn_5Sb_4In_{2-\delta}$. Left: 200 K, orthorhombic RT form. Right: 120 K, monoclinic LT form. The rectangles mark the areas for odd *l* where reflections appear that violate the reflection condition for the c-glide (*h*0*l*: $l = 2n$) present in the RT form. Red arrow heads mark rows with diffuse and additional reflections attributed to intergrown domains of $Zn_9Sb_6In_2$. (b) The crystal structure of $Zn_5Sb_4In_{2-\delta}$ at 200 K (left) and at 120 K (right). For better comparability the RT structure was refined in the monoclinic symmetry of the low-temperature form. The Zn3 split position in the room-temperature form (cf. Figure 3a) is now expressed as a single, elongated atom. Ellipsoids are drawn at a 90% probability (cyan, red, and gray denote Zn, Sb, and In atoms, respectively).

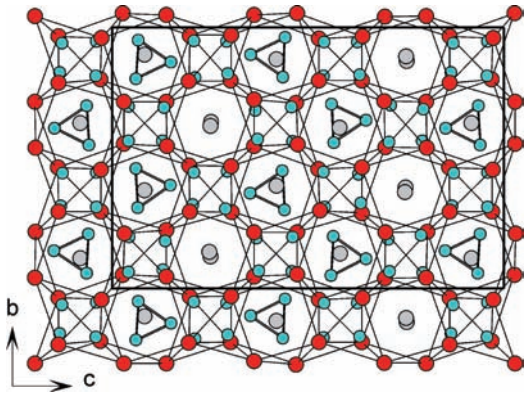

Figure 5. Crystal structure of orthorhombic $Zn_9Sb_6In_2$ projected along the *a* direction [31]. Cyan, red, and gray spheres denote Zn, Sb, and In atoms, respectively.

$Zn_9Sb_6In_2$ is three times that of $Zn_5Sb_4In_{2-\delta}$, and the former structure represents a $(2 \times 3 \times 1)$ superstructure with respect to the tetragonal basis structure of Sb atoms. In the diffraction patterns of $Zn_5Sb_4In_{2-\delta}$ weak and diffuse reflections violate the c-glide extinction conditions and treble the *c* axis (cf. Figure 4a). The intensity of this diffuse scattering is quite independent of the temperature,

and it therefore appears probable that it originates from a minority phase appearing as inclusions in the single crystal. The cell parameters of this phase coincide with those of $Zn_9Sb_6In_2$, and indeed, a multiphase refinement including this phase did yield a better fit to the data. Including the second phase, $Zn_9Sb_6In_2$, leads to an improvement of R1/wR2 to 3.34/6.59 for *all* reflections (cf. Table 1), at a minority component content of 8% (120 K data).

Physical Properties of $Zn_5Sb_4In_{2-\delta}$. In the light of the remarkable thermoelectric properties of binary zinc antimonides an investigation of those properties for $Zn_5Sb_4In_{2-\delta}$ and especially their comparison with the state-of-the-art material Zn_4Sb_3 is interesting. Binary zinc antimonides combine narrow band gaps with complex structures,[9] which is a key for achieving reasonably high Seebeck coefficients S and at the same time low electric resistivities ρ and lattice thermal conductivities κ_L. The thermoelectric efficiency of a material is characterized by the thermoelectric figure of merit $z = S^2/\rho\kappa$ where the total thermal conductivity κ is a sum of an electronic and the lattice contribution, κ_e and κ_L, respectively.[34,35] For β-Zn_4Sb_3 exceptionally low thermal conductivities have been reported,[8] comparable to vitreous materials, and attributed to structural disorder featuring vacancies and interstitial Zn atoms.[18]

Preliminary electronic structure calculations on the monoclinic LT form of $Zn_5Sb_4In_{2-\delta}$ assuming fully occupied In positions ($\delta = 0$) showed a band gap of about 0.3 eV at the Fermi level (see Supporting Information).[36] This indicates that the characteristic feature of zinc antimonides, namely, the realization of narrow band gaps in framework structures with high coordination numbers (>4), [9] is maintained in the ternary derivative.

Figure 6 compiles the resistivity, thermopower, and thermal conductivity of $Zn_5Sb_4In_{2-\delta}$ in comparison with Zn_4Sb_3 in the temperature range between 10 and 350 K.[37] The resistivity of $Zn_5Sb_4In_{2-\delta}$ crystals increase almost linearly with increasing temperature from 1.5 mΩ cm at 10 K until it reaches a maximum at around 220 K (Figure 6a). After this temperature the resistivity decreases exponentially, semiconductor-like, with an estimated activation energy of the order of 0.1 eV. The RT value of ρ is around 2.5 mΩ cm. In contrast, Zn_4Sb_3 displays a metallic temperature behavior of the resistivity throughout the whole temperature range, which however is interrupted by a pronounced discontinuity between 235 and 255 K where two consecutive order−disorder phase transitions take place.[38,39] The resistivity magnitudes (mΩ cm range) of both compounds are typical of poor metals or heavily doped semiconductors. For $Zn_5Sb_4In_{2-\delta}$ this is ascribed to the In deficiency because, as mentioned above, according to electronic structure calculations hypothetical $Zn_5Sb_4In_2$ would represent a narrow gap semiconductor with a completely filled valence band. The resistivity change of $Zn_5Sb_4In_{2-\delta}$ around 220 K raises the suspicion that it is connected to the monoclinic-to-orthorhombic phase transition. However, this temperature is higher than the transition temperature

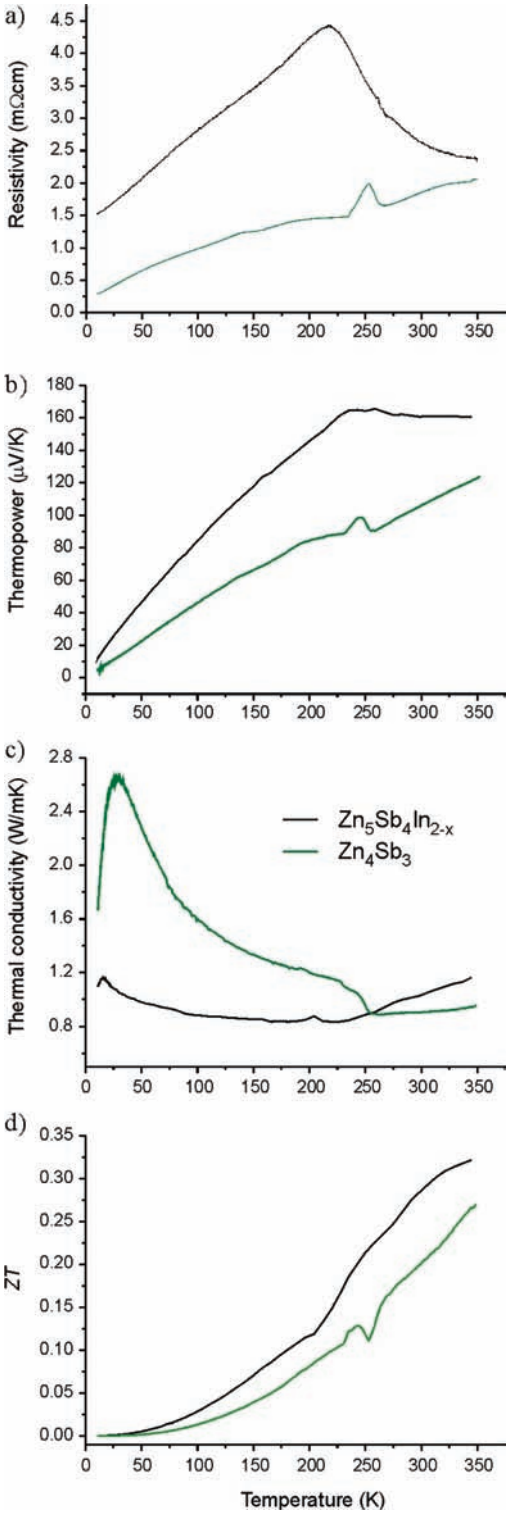

Figure 6. Electrical resistivity (a), thermopower (b), thermal conductivity (c), and the thermoelectric Figure of Merit (d) of $Zn_5Sb_4In_{2-\delta}$ (black lines) in comparison with Zn_4Sb_3 (green lines). Zn_4Sb_3 data are according to ref 38.

(34) *CRC Handbook of Thermoelectrics*; Rowe, D. M., Ed.; CRC Press Inc.: Boca Raton, FL, 1995.
(35) DiSalvo, F. J. *Science* **1999**, *285*, 703.
(36) Electronic structure calculations have been performed with the program package VASP: (a) Kresse, G.; Hafner, J. *Phys. Rev. B* **1993**, *48*, 13115. (b) Kresse, G.; Furthmüller, J. *Comput. Mater. Sci.* **1996**, *6*, 15.
(37) We use the Zn_4Sb_3 data reported in ref 38. Those data adjoin nicely to the original high-temperature data in ref 8.
(38) Wu, Y.; Nylén, J.; Newman, N.; Naseyowma, C.; Garcia-Garcia, F. J.; Häussermann, U. *Chem. Mater.* **2009**, *21*, 151.
(39) Bhattacharya, S.; Hermann, R. P.; Keppens, V.; Tritt, T. M.; Snyder, G. J. *Phys. Rev. B* **2006**, *74*, 134108.

observed in the single crystal diffraction experiment and, more likely, the resistivity maximum is caused by a process of carrier activation which increases either the concentration or the mobility of the dominant charge carriers. To investigate the nature of this phenomenon, Hall and/or reflectivity measurements would be required.

The thermopower S of $Zn_5Sb_4In_{2-\delta}$ exhibits a positive temperature dependence and attains a value of +162 mV/K at around 220 K after which it levels off (Figure 6b). The discontinuity coincides with the temperature where the resistivity attains a maximum. The positive sign of S implies that holes are the majority charge carriers. This is also the case for binary zinc antimonides. The leveling off of S above 220 K is then connected to the proposed carrier activation as discussed for the resistivity change. Also the thermopower of Zn_4Sb_3 increases monotonically with increasing temperature.[38,39] However, the slope is smaller than for $Zn_5Sb_4In_{2-\delta}$ and values are substantially lower. At RT the thermopower of Zn_4Sb_3 is 113 μV/K compared to 160 μV/K for $Zn_5Sb_4In_{2-\delta}$.

As already mentioned, the comparison of the thermal conductivity κ of $Zn_5Sb_4In_{2-\delta}$ and Zn_4Sb_3 is most interesting (Figure 6c). At temperatures between 255 and 350 K Zn_4Sb_3 occurs in its disordered β-form. At 350 K the magnitude of κ is around 0.95 W/mK and decreases slightly upon cooling until around 255 K, where a discontinuous rise occurs at the $\beta-\alpha$ phase transition. Magnitudes of κ around 1 W/mK at RT are typically associated with glass-like materials, for example, κ of vitreous silica is around 1.5 W/mK at 300 K.[40] Over the temperature region of the two phase transitions κ of Zn_4Sb_3 increases by 20−25%.[38,39] Upon further cooling κ rises in a $1/T$ manner until a maximum at around 25 K. This behavior is typical of ordered and well crystallized materials where heat is carried by elastic waves.[41,42] The probability of predominant phonon−phonon Umklapp scattering decreases with decreasing temperature, which leads to an increase of the thermal conductivity. The maximum is reached when the phonon mean free path becomes comparable to the crystal dimension.

The temperature behavior of κ of $Zn_5Sb_4In_{2-\delta}$ is strikingly different. First of all we note that low magnitudes (around 1 W/mK) occur over the whole range of temperatures. The increase of κ with decreasing temperatures characteristic for crystals is absent, or only weakly expressed. Around 200 K the thermal conductivity of $Zn_5Sb_4In_{2-\delta}$ exhibits a hump which is found reproducibly. This hump may be a consequence of the low-temperature order−disorder phase transition of $Zn_5Sb_4In_{2-\delta}$. At temperatures above 220 K κ rises which may be attributed to an increasing contribution κ_e according to the proposed increase of charge carriers at this temperature. The weak temperature dependence and generally low magnitudes of κ for $Zn_5Sb_4In_{2-\delta}$ are puzzling. An explanation for this phenomenon could be the presence of domains of $Zn_9Sb_6In_2$ in $Zn_5Sb_4In_{2-\delta}$.

Finally we discuss the thermoelectric figure of merit in the from of dimensionless $zT = (S^2/\rho\kappa)T$ (Figure 6d). Because of its higher S and low κ, $Zn_5Sb_4In_{2-\delta}$ outperforms Zn_4Sb_3 in the investigated temperature range 10−350 K. However, zT of Zn_4Sb_3 will increase steadily until it reaches 1.3 at 670 K. [8] For $Zn_5Sb_4In_{2-\delta}$ the constant magnitude of S above 220 K is detrimental to zT at higher temperatures. If the mechanism behind the electronic property changes at 220 K could be identified and balanced, $Zn_5Sb_4In_{2-\delta}$ would represent a promising thermoelectric material.

Conclusions

The ternary intermetallic compound $Zn_5Sb_4In_{2-\delta}$ (δ = 0.15(3)) was synthesized and structurally characterized. $Zn_5Sb_4In_{2-\delta}$ features 3^2434 nets of Sb atoms that are stacked in antiposition orientation. This is a prominent structural motif of intermetallic compounds, most notable is the $CuAl_2$ type, where structural variety arises from different fillings of square antiprismatic and tetrahedral voids provided by antiposition stacked 3^2434 nets. However, the Zn distribution in tetrahedral voids of the Sb framework is unusual for $CuAl_2$-type derivatives, and $Zn_5Sb_4In_{2-\delta}$ is rather considered as a derivative of binary zinc antimonides (e.g., ZnSb and Zn_4Sb_3) where rhomboid rings Zn_2Sb_2 are the central structural motif. Similar to binary zinc antimonides $Zn_5Sb_4In_{2-\delta}$ shows promising thermoelectric properties. As a matter of fact, its thermoelectric figure of merit between 10 and 350 K is higher than that of the state-of-the-art thermoelectric Zn_4Sb_3. Especially the very low thermal conductivity down to LTs is noteworthy. The noncrystalline behavior of the temperature dependency of thermal conductivity is attributed to the presence of domains of a second phase, $Zn_9Sb_6In_2$, in crystals of $Zn_5Sb_4In_{2-\delta}$. The electrical resistivity and thermopower of $Zn_5Sb_4In_{2-\delta}$ are typical of a heavily doped or degenerate semiconductor. Both properties change discontinuously at around 220 K. The change in resistivity appears as a metal-to-semiconductor transition, and its nature is not yet understood.

Acknowledgment. This work was supported by the Swedish Research Council (VR) and the National Science Foundation through Grant DMR-0638826. We are grateful to Dr. Gordon Moore, ASU, for assistance with the microprobe analysis.

Supporting Information Available: Crystallographic data in CIF format for $Zn_5Sb_4In_{2-\delta}$ (RT and LT form) and $Zn_9Sb_6In_2$, density of states for $Zn_5Sb_4In_2$ (δ = 0). This material is available free of charge via the Internet at http://pubs.acs.org.

(40) Damon, D. H. *Phys. Rev. B* **1973**, *8*, 5860.
(41) Slack, G. A. In *Solid State Physics*; Ehrenreich, H.; Seitz, F.; Turnbull D., Eds.; Academic Press: New York, 1979; Vol. 34, pp 1−71.
(42) *Thermal Conductivity: Theory, Properties and Applications*; Tritt, T. M., Ed.; Springer: New York, 2004.